

Inverse Compton Scenarios for the TeV Gamma-Ray Emission of the Galactic Centre

J. A. Hinton

*Max-Planck-Institut für Kernphysik, P.O. Box 103980, D 69029 Heidelberg, Germany
Landessternwarte, Universität Heidelberg, Königstuhl, D 69117 Heidelberg, Germany*

F. A. Aharonian

Max-Planck-Institut für Kernphysik, P.O. Box 103980, D 69029 Heidelberg, Germany

ABSTRACT

The intense Compton cooling of ultra-relativistic electrons in the Klein-Nishina regime in radiation dominated environments, such as that found in the Galactic Centre, may result in radically different electron spectra than those produced by Synchrotron cooling. We explore these effects and their impact on the X-ray and γ -ray spectra produced in electron accelerators in this region in comparison to elsewhere in our galaxy. We discuss the broad-band emission expected from the newly discovered pulsar wind nebula G 359.95–0.04 and the possible relationship of this X-ray source to the central TeV γ -ray source HESS J1745–290. Finally we discuss the possible relationship of the Galactic Centre INTEGRAL source IGR J1745.6–2901 to the TeV emission.

Subject headings: pulsar wind nebulae: general — pulsar wind nebulae: individual(G 359.95–0.04, G 0.9+0.1)

1. Introduction

The detection of TeV γ -rays from the Galactic Centre (GC) by several groups, Kosack et al. (2004); Tsuchiya et al. (2004); Aharonian et al. (2004b); Albert et al. (2006), can be considered as one of the most exciting discoveries of recent years in High Energy Astrophysics. After initial disagreements, the basic properties of the TeV source (HESS J1745–290) now seem to be firmly established, with the values from the H.E.S.S. (Hinton et al. 2004) instrument providing the highest level of accuracy. The key experimental findings are:

- The energy spectrum in the range 0.15–20 TeV can be described by a power law: $dN/dE = k(E/1\text{TeV})^{-\Gamma} \text{ cm}^{-2} \text{ s}^{-1} \text{ TeV}^{-1}$ with $k = 1.8 \pm 0.1_{stat} \pm 0.3_{sys}$, $\Gamma = 2.29 \pm 0.05_{stat} \pm 0.1_{sys}$ (Rolland & Hinton 2005).
- There is no evidence for variability on hour to year time-scales (Rolland & Hinton 2005; Albert et al. 2006)

- The centroid of the γ -ray emission lies within $1'$ of Sgr A* (Aharonian et al. 2004b; Rolland & Hinton 2005)
- The rms size of the emission region must be less than $3'$, equivalent to 7 parsecs at the GC distance (Aharonian et al. 2004b)

The implied 1–10 TeV γ -ray luminosity of the source is $10^{35} \text{ erg s}^{-1}$. A wide range of possible counterparts and mechanisms have been put forward to explain the γ -ray emission. These include the annihilation of dark matter (unlikely due to the measured spectral shape, see Profumo (2005)) and the astrophysical objects Sgr A* (Aharonian & Neronov 2005) and Sgr A East (Fatuzzo & Melia 2003; Crocker et al. 2005). A hadronic origin of the γ -ray emission seems plausible, originating either within these sources or indirectly via the injection of hadrons into the dense central parsec region (Aharonian & Neronov 2005; Lu et al. 2006; Liu et al. 2006). Indeed, there is strong evidence

for the existence of a proton accelerator close to the GC (at least in the past) to explain the recently discovered TeV emission of the GMCs of the central molecular zone (Aharonian et al. 2006). Nevertheless, an origin of the central $\leq 0.1^\circ$ γ -ray emission in the interactions of TeV electrons remains a compelling alternative. Several scenarios have been discussed in which the persistent TeV emission is explained by inverse Compton (IC) scattering of electrons in the central parsec. The termination shock of a hypothetical wind from the supermassive black hole (Atoyan & Dermer 2004), stellar wind shocks (Quataert & Loeb 2005) and the newly discovered X-ray nebulae $8''$ from Sgr A* (Wang et al. 2006) have all been proposed as acceleration sites for these electrons.

Whilst the formation of synchrotron and IC nebulae around sources of multi-TeV electrons proceeds in general in the GC as in other regions of the galactic disk (GD), the very high density of low-frequency radiation in GC leads to significant deviations from the typical disk scenario. The high radiation density (out to ~ 10 pc from Sgr A*) not only provides copious targets for γ -ray production, but also creates rather unusual conditions for the formation of the spectrum of TeV electrons. For magnetic fields less than $\sim 100 \mu\text{G}$, the energy density of radiation appears much higher than the energy density of the magnetic field, thus even in the modest Klein-Nishina (KN) regime, TeV electrons are cooled predominantly by IC losses. This leads to *hardening* of the spectrum (not steepening as in the typical GD environment) up to very high (≥ 100 TeV) energies (the deep KN regime), where the synchrotron losses start to dominate over IC losses. Figure 1 illustrates the cooling time for electrons in the presence of both strong radiation fields and magnetic fields (lower panel) and the modification of the injected electron spectrum after cooling (upper panel). The time-evolution of the electron spectrum (in Figure 1 and throughout this paper) is calculated numerically, considering energy losses and injection of electrons in time-steps much shorter than the age of the system. Synchrotron and IC energy losses are calculated using the formalism developed by Blumenthal & Gould (1970).

The irregular spectral shape of electrons shown in Fig. 1 is reflected differently in the synchrotron and IC radiation components (see e.g.

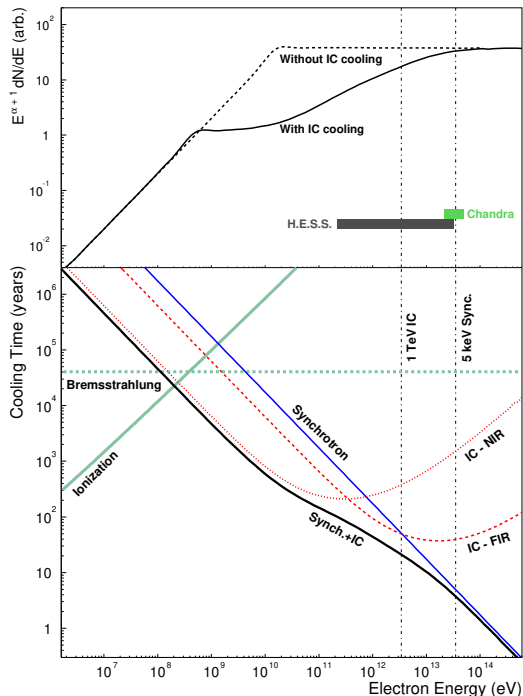


Fig. 1.— Top panel: energy spectrum of electrons with continuous injection with $dN/dE \propto E^{-\alpha}$ (with $\alpha = 1.8$) and cooling over a 10^4 year period. The dashed line shows the cooled spectrum for electrons suffering only synchrotron losses (for $B = 120 \mu\text{G}$). The solid line shows the spectrum after synchrotron and IC cooling on radiation fields typical of the central parsec of our galaxy. The shaded regions show the range of electron energies contributing to signals seen in the energy ranges of the Chandra and H.E.S.S. instruments. Bottom panel: cooling time via IC (dashed lines, FIR and optical radiation fields) and synchrotron radiation (solid blue line). The lower heavy line shows the overall cooling time for IC and synchrotron radiation. The approximate energy loss time-scales for ionisation and bremsstrahlung (in a neutral environment of number density 1000 cm^{-3}) are shown for comparison.

Khangulyan & Aharonian 2005; Moderski et al. 2005). Another interesting feature of these conditions is that due to enhanced IC losses, the synchrotron radiation of electrons will be strongly suppressed (by an order of magnitude or more), unless the magnetic field in extended regions of GC exceeds $100 \mu\text{G}$. This situation is in stark contrast to that in the GD, where IC emission is strongly suppressed for magnetic fields $> 10 \mu\text{G}$. In Fig. 2, we compare the fractional energy distribution resulting from the injection of the same power-law spectrum of electrons for two values of the mean magnetic field in the source ($10 \mu\text{G}$ and $100 \mu\text{G}$) for 3 locations in our galaxy: (i) the central 1 pc, (ii) at 100 pc from GC, and (iii) in a standard site in the GD. The radiation fields used in Fig. 2 and throughout this paper are given in Table 1.

Some of these effects have been discussed by Wang et al. (2006) in the context of a possible identification of HESS J1745–290 with the candidate Pulsar Wind Nebula (PWN) G 359.95–0.04. In this paper, we present the results of numerical calculations based on time-dependent treatment of the formation of the energy spectrum of electrons. We discuss the case of G 359.95–0.04 and show that indeed this PWN can explain the TeV γ -ray emission from the GC. The implied B -field in this scenario appears to be around $100 \mu\text{G}$. Remarkably, PWNe similar to G 359.95–0.04 (i.e. with similarly large B -field and comparable energetics) located in the conventional sites within the GD would be undetectable with any current or planned TeV γ -ray instrument. The converse also holds: typical TeV γ -ray PWNe (with B -field of about $10 \mu\text{G}$ or less) would not be detectable in X-rays if located in the central 1 pc region. Finally, we discuss the conditions implied by the interpretation of the hard X-ray emission detected by INTEGRAL (Neronov et al. 2005; Bélanger et al. 2005) as synchrotron emission of multi-TeV electrons in the context of the severe IC losses of these electrons.

2. Pulsar Wind Nebulae

Pulsar Wind Nebulae are perhaps the most efficient astrophysical particle accelerators in our galaxy. The best studied PWN, the Crab Nebula, accelerates electrons up to $\sim 10^{16}$ eV despite the

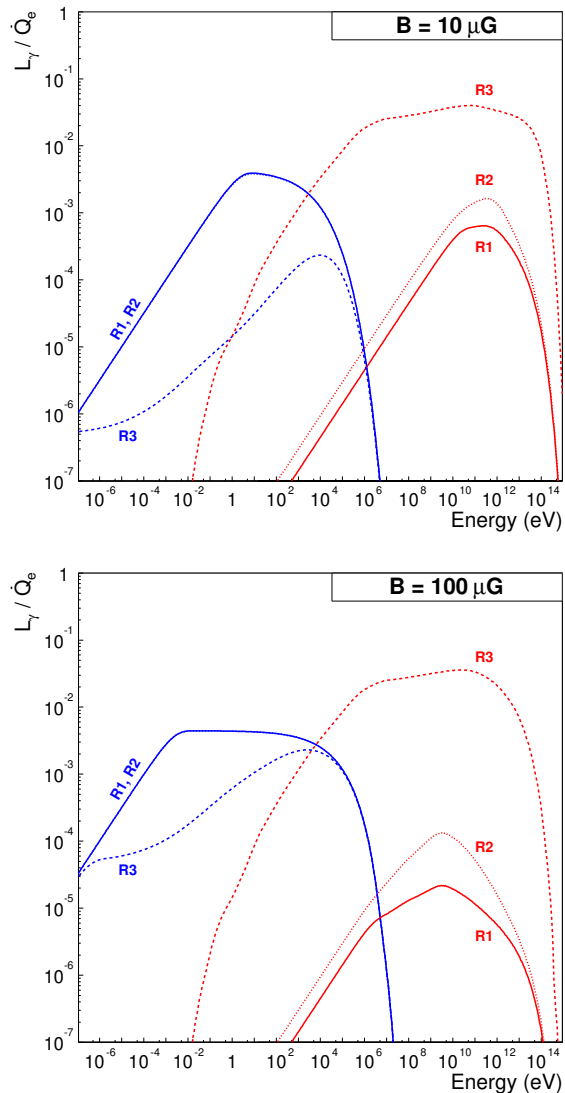


Fig. 2.— Fraction of the total power injected in electrons radiated in different spectral bands for $B = 10 \mu\text{G}$ (top) and $B = 100 \mu\text{G}$ (bottom). In each case three radiation fields are considered: R1, a typical galactic disk environment; R2, ~ 100 pc from the GC and R3, within the central parsec. Continuous injection (over a 10^4 year period) with $dN/dE \propto E^{-2}$ and an exponential cut-off at 200 TeV are assumed in all cases. The synchrotron curve for R2 lies underneath that for R1.

Rad. Field / Component (kT)	UV/optical (3 eV)	NIR (0.3 eV)	FIR (6×10^{-3} eV)	CMBR (2.35×10^{-4} eV)
R1	-	0.2	0.2	0.26
R2	-	9	1	0.26
R3	5000	5000	500	0.26
R4	50	50	5	0.26

Table 1: Energy density (in eV cm^{-3}) of the thermal components of radiation fields used for the calculation of electron cooling and γ -ray production via inverse Compton scattering. Field R1 represents the typical galactic disk environment. R2 reflects the situation in the inner ~ 100 pc and R3 is a model of the intense field of the central cubic parsec of our galaxy. R4 is a scaled down version of R3 to approximate the situation 10 pc from the GC.

rapid synchrotron losses of these particles in its 160 μG magnetic field (Aharonian et al. 2004a). The recent detections of extended TeV emission from several PWNe, including MSH-15-52 (Aharonian et al. 2005b) and G 18.0-0.7/HESS J1825-137 (Aharonian et al. 2005c) with the H.E.S.S. instrument suggest that such objects are copious TeV γ -ray emitters. In this context, a PWN may provide a natural explanation for the GC TeV emission. Here we discuss, in detail, the case of the new PWN candidate G 359.95-0.04.

2.1. The case of G 359.95-0.04

The X-ray nebula G 359.95-0.04 was discovered in deep Chandra observations of the Galactic Centre (Wang et al. 2006) and lies at a projected distance to Sgr A* of 0.3 pc. The nebula exhibits a cometary morphology with a projected size of 0.07×0.3 pc. The overall energy spectrum of this object is purely non-thermal, with a power-law index of $1.94^{+0.17}_{-0.14}$ and an unabsorbed 2–10 keV X-ray luminosity of $\approx 10^{34}$ erg/s. The Chandra data reveal a softening of spectral index with distance from the “head” of the nebula, a possible signature of cooling of electrons away from the accelerator. Wang et al. (2006) have suggested that the head of the nebula contains a young pulsar and that G 359.95-0.04 is likely a ram-pressure-confined PWN.

G 359.95-0.04 lies within the 68% confidence error circle of the γ -ray source HESS J1745-290. The possible connection between these two objects was pointed out by Wang et al. (2006), who discuss in some detail the important physical aspects involved in the relationship between the X-

ray and γ -ray emission. One of our aims here is to make a full time-dependent calculation to investigate more deeply the likelihood of an association of these two objects. A major difficulty in such an association is the $\sim 0.1^\circ$ angular resolution of H.E.S.S. In this scenario, the γ -ray signal would be point-like and non-variable and the only available information for modelling is the spectral data in the X-ray and γ -ray bands. However, the X-ray morphology provides some clues to the environment of the PWN. For example, the fact that X-ray spectrum softens rather than hardens away from the (nominal) pulsar position indicates that the X-ray emitting electrons are cooled by synchrotron radiation (or IC radiation in the Thompson regime) rather than by IC radiation in the Klein-Nishina (KN) regime as might be expected in the dense GC radiation fields. This fact alone places a lower limit on the magnetic field in the PWN of $\sim 100 \mu\text{G}$.

Due to KN suppression, it is likely that the dominant target for IC radiation at a few TeV is the far infrared background. Matching the flux of HESS J1745–290 at these energies with a nominal FIR radiation energy density of 5000 eV cm^{-3} (Davidson et al. 1992) requires a B -field of $\sim 120 \mu\text{G}$. In the case that HESS J1745–290 and G 359.95-0.04 are *not* associated, this value provides a lower limit on the average magnetic field in the PWN. Fig. 3 shows a model spectral energy distribution (SED) for G 359.95–0.04 with IC on a FIR field. The injection spectrum of electrons is assumed to be of the form $dN/dE \propto E^{-\alpha} e^{-E/E_0}$ with $\alpha = 1.8$ and $E_0 = 200 \text{ TeV}$. A source age of 10^4 years is assumed and a total power of 7.4×10^{35} erg/s injected into relativistic electrons is required

to match the measured X-ray flux (assuming a distance to the galactic centre of 7.6 ± 0.4 pc (Eisenhauer 2005)). As the cooling time of the electrons responsible for the observed X-ray and γ -ray emission is much shorter than the age of the pulsar in this scenario, possible evolutionary effects on the injection power (related to the breaking of the pulsar spin) can safely be neglected, we therefore assume a constant injection rate in the simulations presented here. Fig. 3 demonstrates an important aspect of IC cooling: the KN effect acts twice on the IC spectrum (firstly by distortion of the electron spectrum through cooling, and secondly in the production of IC emission), but only once on the Synchrotron spectrum. This means that the hardening effect of cooling in the KN regime is masked in the IC spectrum but clearly visible in the Synchrotron emission.

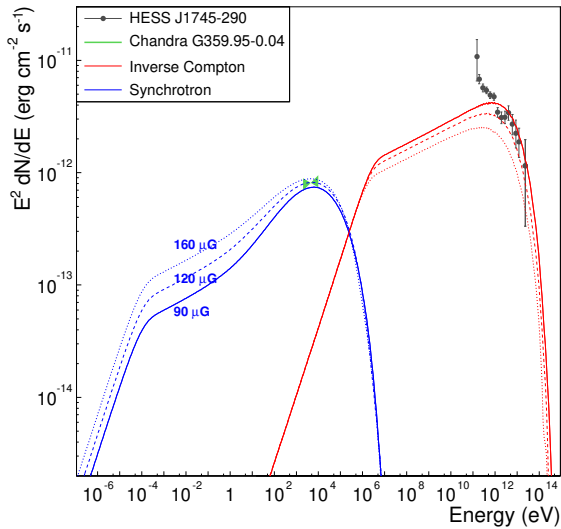


Fig. 3.— Spectral energy distribution for inverse Compton scattering on a single temperature FIR radiation field of density 5000 eV cm^{-3} . The three line styles indicate the effect of changing magnetic field strength (with all other parameters fixed). The assumed injection spectrum is described in the main text. H.E.S.S. data are taken from (Rolland & Hinton 2005), Chandra data from (Wang et al. 2006).

The effect of adding different temperature components to the GC radiation field is shown in Fig. 4. Optical ($kT = 0.3 \text{ eV}$), and ultraviolet

($kT = 3.0 \text{ eV}$) energy densities of $5 \times 10^4 \text{ eV cm}^{-3}$ are assumed, consistent with the values expected within the central parsec of our galaxy (Davidson et al. 1992). The injected electron spectrum is identical to that in Fig. 3. On such a compound field, low energy electrons are cooled by IC scattering on optical seed photons, with higher energies cooled by IC on the FIR. This effect leads to rather different shapes for the IC spectra from these two components. It can be seen in this figure that the contribution of UV is likely to be small because of strong KN suppression. This optical/UV domain can in principle be explored by the GLAST satellite (Thompson 2004), but such measurements may be rather difficult due to the strong diffuse background and the modest angular resolution of the instrument.

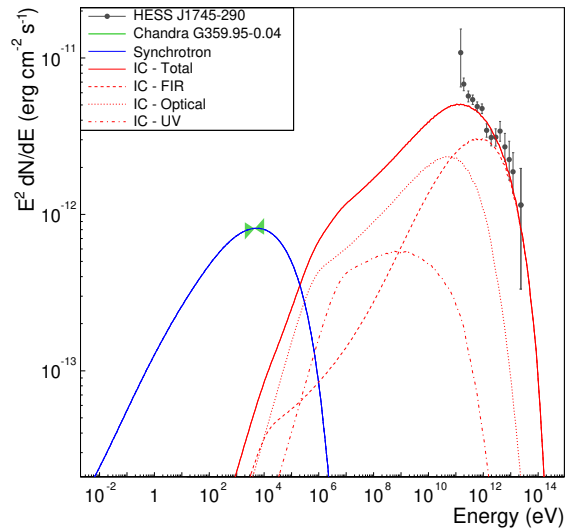


Fig. 4.— Spectral energy distribution for a realistic GC radiation field with FIR, optical and UV components. The magnetic field strength is fixed at $120 \mu\text{G}$. Details are given in the main text.

The spectral and spatial distribution of low energy electrons in the PWN can in principle be traced using radio observations. However, no point-like or extended source is observed at the position of G 359.95-0.04 in 6 cm observations and a three sigma energy flux upper limit of $5 \times 10^{-17} \text{ erg cm}^{-2} \text{ s}^{-1}$ has been derived (Yusef-Zadeh 2006). This limit lies almost three orders of magnitude below the curve shown in Fig. 3. There are two

factors which may both act to mitigate this apparent contradiction:

1. the electron energy spectrum has a low energy cut-off. Figure 5 shows the impact of a low energy cut-off in the electron spectrum on the IC and synchrotron spectra. If the radio emission region is considered to be identical to that of keV X-rays (see point 2 below) then there is an implied low energy cut-off at ~ 1 TeV and rather poor agreement with the lowest energy γ -ray data points. Indeed a low energy cut-off in the electron spectrum is expected within the PWN paradigm. For example, in the case of the Crab Nebula, Kennel & Coriniti (1984) suggest a minimum injection energy of ~ 1 TeV at the wind termination shock. Wang et al. (2006) suggested a minimum low energy cut-off of at 5 GeV derived from the radio data available at that time.
2. the cooling time of the radio emitting electrons is almost three orders of magnitude longer than that of the X-ray emitting electrons. Depending on the transport mechanism of particles in the nebula the angular diameter of the radio emission may be expected to be much larger than the X-ray nebula and with correspondingly lower surface brightness. We envisage two general transport scenarios: a) *energy independent advection*. In this case the PWN size is inversely proportional to the cooling time of electrons and the ratio of radio to X-ray angular size is ~ 1000 and the flux within the bounds of the X-ray nebula is a factor of 10^6 lower than that presented in figures 4 and 5. Clearly there is no contradiction to the radio limit in this case. b) *diffusion* with $D \propto E^\alpha$ and $r = \sqrt{2Dt}$. In this case the PWN size is proportional to $\sqrt{E^\alpha/t_{\text{cool}}}$. For a value of $\alpha = 0.5$ the expected ratio of radio to X-ray size is ~ 3 (implying a one order of magnitude reduction in surface brightness). In this case a low energy cut-off at ~ 50 GeV is still required. Larger values of α (for example Bohm diffusion, $\alpha = 1$) appear to be excluded by the observed energy dependant morphology at X-ray wavelengths.

Regardless of the nature of the TeV source, it

seems that one or both of these effects must occur to explain the radio to X-ray behaviour of G 359.95-0.04.

As is clear from Fig. 1, Bremsstrahlung losses are unlikely to be important in the PWN as the ambient density is likely $\ll 1000 \text{ cm}^{-3}$.

Fig. 1 (top panel) illustrates the electron energies contributing to the H.E.S.S. and Chandra signals for a $120 \mu\text{G}$ magnetic field. As the γ -ray emission takes place predominantly in the KN regime, the energy range of electrons probed by H.E.S.S. is extended by an order of magnitude relative to the Thompson regime case. In contrast, the narrow energy range probed by Chandra reflects the standard $\epsilon_\gamma \propto \sqrt{\epsilon_e}$ case. As synchrotron emission below 1 keV is heavily absorbed in the GC, VHE γ -ray emission represents the *only* way to study the 200 GeV – 20 TeV electrons. From the lower panel of Fig. 1 it is apparent that the X-ray emitting electrons have extremely short lifetimes (~ 5 years). This fact, coupled with the known size of the PWN in X-rays (~ 0.3 pc), implies that the propagation speed of electrons downstream from the pulsar should be approximately 20% of the speed of light, consistent the expectations for PWN (see for example Blondin et al. (2001) and Kennel & Coriniti (1984)).

It is clear from Fig. 4 that the shape of the H.E.S.S. and Chandra spectra can be explained in broad terms in this scenario. G 359.95–0.04 may produce ~ 100 GeV γ -rays very efficiently despite its high B -field. Fine-tuning of the model and adjustment of radiation fields would be required to fit all H.E.S.S. spectral data points but we consider such tuning unjustified given the possibility of the contribution of other sources (the supernova remnant Sgr A East, Sgr A*, etc) to the H.E.S.S. signal, and since there are larger systematic errors on the H.E.S.S. spectrum close to threshold. It therefore appears that G 359.95-0.04 is a promising counterpart to the TeV GC source. As can be seen from Fig. 2, a PWN like G 359.95–0.04 could not be detected by any current or planned γ -ray detector if located in a standard region of the galactic disc. The existence of extended regions with comparable radiation densities outside of the GC, for example in the central regions of young stellar clusters, seems unlikely since ~ 1000 O-stars would be required within 1 cubic parsec to reach this energy density.

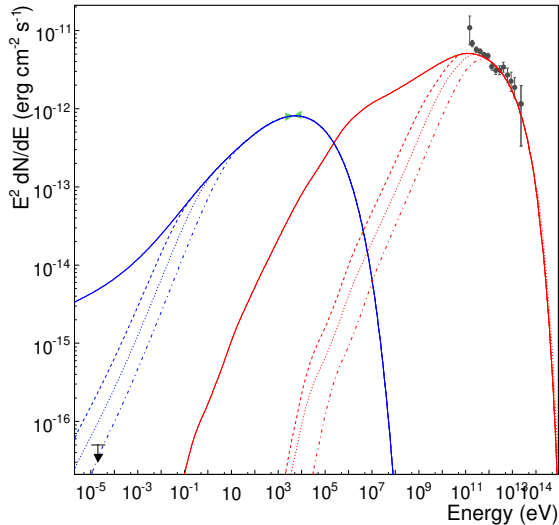


Fig. 5.— As for Fig 4 but showing the effect of a low energy cut-off in the injected electron spectrum (and with an expanded flux scale). The corresponding minimum energies are 1 MeV (solid line), 100 GeV (dashed line), 300 GeV (dotted line) and 1 TeV (dot-dashed line). A 6cm radio flux upper limit for G 359.95-0.04 from Yusef-Zadeh (2006) is shown.

2.2. Comparison with G 0.9+0.1

G 0.9+0.1 is a composite SNR with a bright radio shell and a compact core (Helfand & Becker 1987). The central object was identified as a PWN based on its X-ray properties (Mereghetti et al. 1998; Porquet et al. 2003). γ -ray emission associated with the PWN has been reported by the H.E.S.S. collaboration (Aharonian et al. 2005a), with energy flux comparable to that emitted in X-rays ($\sim 3 \times 10^{-12} \text{ cm}^{-2} \text{ s}^{-1}$). The PWN in G 0.9+0.1 can be considered an intermediate case between a ‘standard’ disk PWN and G 359.95-0.04. With a projected distance from GC of 100 pc, radiation fields close to G 0.9+0.1 are likely a factor 10–100 higher than local densities, as represented by radiation field R2 in Table 1 (see for example Moskalenko et al. 2006). Indeed an increased energy density of 8 eV cm^{-3} in optical photons was invoked in Aharonian et al. (2005a)

where a time-independent IC model¹ was fit to the X-ray and γ -ray data. Here we revisit the SED of G 0.9+0.1 from the perspective of a time-dependent evolution of the electron spectrum. In the following we assume that G 0.9+0.1 is located at the same distance as the GC (7.6 kpc).

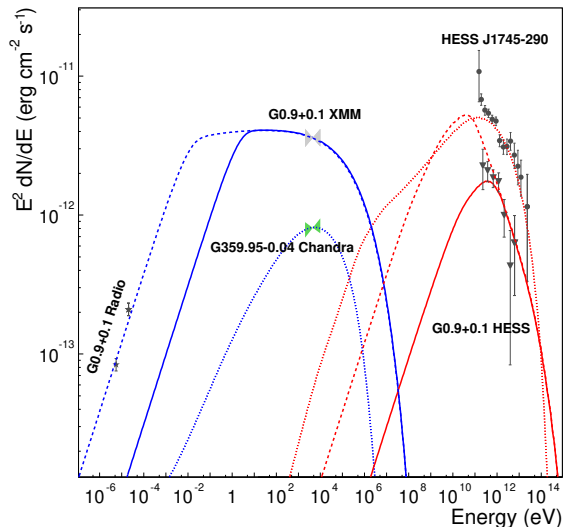


Fig. 6.— Comparison of the G 359.95-0.04 SED shown in Fig. 4 (dotted model curves) with G 0.9+0.1 (solid and dashed curves). The solid and dashed curves differ only the assumed age of the source. Model parameters are given in the main text. Radio data are taken from Helfand & Becker (1987), XMM data from Porquet et al. (2003).

Using values of the optical and FIR densities of 9 eV cm^{-3} and 1 eV cm^{-3} respectively, as suggested by (Moskalenko et al. 2006) for the wider GC region, we find that a model with $\alpha = 2$, $L_e = 7 \times 10^{36} \text{ erg/s}$, $B = 10 \mu\text{G}$ and a pulsar age of 8 ky, is consistent with the H.E.S.S. and X-ray data (see Fig. 6). This value is close to the 6800 year age of the remnant estimated assuming expansion in the Sedov phase (Mereghetti et al. 1998). Pulsar ages much shorter than 8 ky are excluded by the absence of a spectral maximum (produced by a cooling break in the electron spectrum) within the H.E.S.S. energy range. Recently,

¹i.e. a model for the present-day electron spectrum without consideration of the injection spectrum required to produce such a spectrum after cooling

Porter et al. (2006) have fit the ‘prompt’ electron spectrum of G 0.9+0.1 using the radiation field of Moskalenko et al. (2006) and derive a magnetic field of $B = 9.5 \mu\text{G}$ very close (as expected) to the value given here.

A second component of lower energy electrons is required to explain the radio emission (Helfand & Becker 1987) unless an age of $\approx 1.3 \times 10^5$ years is assumed (see dashed line on Fig. 6). Sidoli et al. (2000) used the break energy implied by the combination of radio and X-ray data to estimate the age of the pulsar to be ~ 3000 years (assuming $B = 67 \mu\text{G}$). The much larger age derived here is a consequence of the lower magnetic field value established by the combination of X-ray and γ -ray data.

3. A central 10 parsec source

The recently detected hard (20–100 keV) X-ray source IGR J1745.6–2901 (Bélanger et al. 2004), is located within $1'$ of Sgr A* and coincident with HESS J1745–290. The angular resolution of INTEGRAL ($12'$ FWHM) is comparable with that of H.E.S.S. and similar difficulties exist with the identification of a counterpart. However, a combination of the INTEGRAL data with that of XMM suggests that the INTEGRAL source represents the sum of the emission of the central ~ 20 parsecs, either from a diffuse component or the combination of several discrete sources (Neronov et al. 2005; Bélanger et al. 2005). The combined XMM/INTEGRAL X-ray spectrum of the central region has been derived by both groups, but with somewhat different results. Neronov et al. (2005) provide a broken power-law fit with $\Gamma_1 = 1.85^{+0.02}_{-0.06}$ and $\Gamma_2 = 3.3 \pm 0.1$ with a break at 26 ± 1 keV (BPL). Bélanger et al. (2005) provide a broken power-law fit: $\Gamma_1 = 1.51^{+0.06}_{-0.09}$ and $\Gamma_2 = 3.22^{+0.34}_{-0.30}$ with a break at $27.1^{+2.8}_{-4.4}$ keV and also a cut-off power law fit: $\Gamma = 1.09^{+0.03}_{-0.05}$, $E_{\text{cut}} = 24.38^{+0.55}_{-0.76}$ keV (PLEC). Of these three fits, BPL and PLEC represent the extremes and are used here to illustrate the impact of the X-ray spectral shape on the interpretation. If this emission has a synchrotron origin, then the broken power-law fit suggests a change in the electron spectral slope of ~ 3 , incompatible with the effects of cooling or escape, and with standard acceleration scenarios. It therefore seems that the INTEGRAL data repre-

sent the end of the X-ray spectrum of this object or objects. Fig. 7 shows approximate error boxes corresponding to the spectral fits BPL and PLEC. The difference in low energy slope of these two fits has important implications for the interpretation of this signal in a synchrotron scenario. In either case an abrupt end to the electron spectrum is required to produce an exponential cut-off in the synchrotron spectrum. The PLEC fit implies an extremely hard electron spectrum.

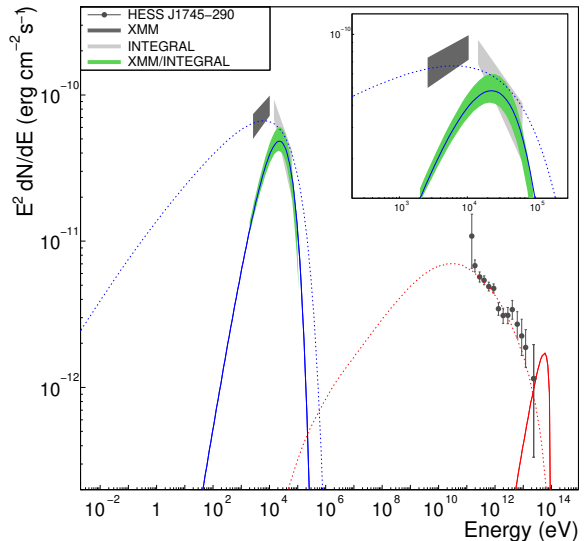


Fig. 7.— Spectral energy distribution for a central 10 pc XMM/INTEGRAL/H.E.S.S. source. Separate XMM and INTEGRAL data are taken from (Neronov et al. 2005), the combined XMM/INTEGRAL fit is that of Bélanger et al. (2005). Model curves are shown for two scenarios: a very young source with $B = 50 \mu\text{G}$, electron spectrum with $\alpha = 0.3$ and a sharp cut-off at 100 TeV (solid curve), an old source with $B = 110 \mu\text{G}$ and an injection spectrum with $\alpha = 1.5$ and an exponential cut-off at 200 TeV (dashed curve). The inset panel provides an expanded view of the X-ray part of the SED.

Although considerable uncertainty exists in the radiation density ~ 10 pc from the GC, it seems likely that the average energy density within the 40 pc diameter INTEGRAL source is roughly two orders of magnitude lower than that within the central parsec (see for example Yusef-Zadeh et al. 1996). For the calculation of the inverse Compton emission we therefore assume the radiation

field R4 given in Table 1. With this radiation density, the association of HESS J1745-290 with IGR J1745.6-2901 implies a B -field of $\sim 100 \mu\text{G}$. In the case that these objects are not associated this B -field can be considered as lower limit on the mean value within the source or sources contributing to the INTEGRAL signal. Conversely if the γ -ray emission has an inverse Compton origin within a 10 pc scale source then the B -field in this region must be $< 100 \mu\text{G}$ to avoid over-producing synchrotron emission. For a $100 \mu\text{G}$ magnetic field, 20 keV synchrotron photons are produced by ~ 70 TeV electrons. The cooling time of these electrons in such a field is extremely short (~ 4 years). The time required for electrons to diffuse out of the central 10 parsecs is comparable (~ 10 years) if a diffuse coefficient close to that appropriate for 70 TeV galactic cosmic rays is assumed (i.e. $D \approx 6 \times 10^{30} \text{ cm}^2 \text{ s}^{-1}$). It therefore seems rather difficult to produce a truly diffuse 20 pc source with such rapid energy losses. This cooling-time was previously discussed by Neronov et al. (2005). A model similar to that of Quataert & Loeb (2005), with acceleration occurring at stellar wind shocks, could avoid this problem by distributing the acceleration sites of electrons over the emission region.

Fig. 7 shows two model curves illustrating the relationship between the X-ray and γ -ray emission. The first (solid) line matches the PLEC fit to the X-ray spectrum but can explain only the highest energy H.E.S.S. points. This scenario requires both an extremely young source (to avoid a cooled spectrum in the XMM domain) and a very hard injection spectrum. The second curve (dashed line) is similar to that given in Neronov et al. (2005) and provides marginal agreement to the BPL fit and reasonable agreement with the H.E.S.S. spectral data. The dramatic difference between these two scenarios illustrates the importance of better constraints on the X-ray spectrum and highlights the value of combined X-ray/ γ -ray measurements.

4. Summary

The central ~ 10 pc of our galaxy provides a unique environment in which high radiation energy densities lead to efficient inverse Compton γ -ray production, and also, due to the Klein-

Nishina effect, to substantial modifications to the form of cooled electron spectra. This region appears to be the only location in our galaxy in which pulsar wind nebulae with high magnetic fields and moderate spin-down luminosities can produce detectable γ -ray emission. In this context, the candidate PWN G 359.95–0.04 provides a plausible counterpart to the γ -ray source HESS J1945–290. The interpretation of IGR J1745.6–2901 and HESS J1945–290 in terms of synchrotron/IC emission in a diffuse 20 parsec source is difficult due to the rapid energy losses of electrons in the region, but remains a viable alternative hypothesis. Finally, hadronic models for the TeV emission, while beyond the scope of this paper, provide equally viable explanations for the current experimental data. Improved γ -ray data should be available in the medium term from the GLAST (Thompson 2004) and H.E.S.S. Phase-2 (Punch 2005) instruments and will provide important constraints on the origin of the high energy emission.

JAH acknowledges the support of the German BMBF through Verbundforschung Astro-Teilchenphysik (05CH5VH1/0). We are grateful to Farhad Yusef-Zadeh for providing a radio upper limit for G 359.95-0.04. We would also like to thank Mitya Khangulyan for many useful discussions and Karl Kosack for his careful reading of the manuscript.

REFERENCES

- Aharonian, F. A., et al. (HEGRA coll.), 2004a, *ApJ*, 614, 897
- Aharonian, F. A., et al. (H.E.S.S. coll.) 2004b, *A&A*, 425, L13
- Aharonian, F. A., et al. (H.E.S.S. coll.) 2005a, *A&A*, 432, L25
- Aharonian, F. A., et al. (H.E.S.S. coll.) 2005b, *A&A*, 435, L17
- Aharonian, F. A., et al. (H.E.S.S. coll.) 2005c, *A&A*, 442, L25
- Aharonian, F. A., et al., (H.E.S.S. coll.) 2006, *Nature*, 439, 695

- Aharonian, F. A. & Neronov, A., 2005, *Astrophys. & Space Science*, 300, 255
- Albert, J., et al., 2006, *ApJ*, 638, L101
- Atoyan, A.M., Dermer, C.D., 2004, *ApJ*, 617, L123
- Bélangier G., Goldwurm A., Goldoni P., et al. 2004, *ApJ*, 601, L163
- Bélangier, G., et al., 2006, *ApJ*, 636, 275
- Blondin, J.M., Chevalier, R.A., Frierson, D. M. 2001, *ApJ*, 563, 806
- Blumenthal, G.R., Gould, R.J., 1970, *RvMP*, 42, 237
- Crocker, R. M., et al., 2005, *ApJ*, 622, 892
- Davidson, J. A., et al., 1992, *ApJ*, 387, 189
- Eisenhauer et al., 2005, *ApJ*, 628, 246
- Fatuzzo, M. & Melia, F. 2003, *ApJ*, 596, 1035
- Hinton, J. A. (for the H.E.S.S. collaboration) 2004, *New Astron. Rev.*, 48, 331
- Helfand, D. J., Becker, R. H., 1987, *ApJ*, 314, 203
- Kennel, C. F. & Coriniti, F. V., 1984, *ApJ*, 283, 710
- Khangulyan, D. & Aharonian, F. A., 2005, in *Proc. "High Energy Gamma-Ray Astronomy"* (Heidelberg, 2004), AIP Conference Proceedings (New York), vol. 745, pp 359
- Kosack, K., et al., 2004, *ApJ*, 608, L97
- Liu, S., Melia, F., Petrosian, V, Fatuzzo, M. 2006, *ApJ*, 647, 1099
- Lu, Y., Cheng, K. S., Huang, Y. F. 2006, *ApJ*, 641, 288
- Mereghetti, S., Sidoli, L. & Israel 1998, *A&A*, 331, L77
- Moderski R., Sikora M., Coppi P., Aharonian F., 2005, *MNRAS*, 363, 954
- Moskalenko, I.V., Porter, T. & Strong, A.W., 2006a, *ApJ*, 640, 155
- Neronov, A., et al., 2005, preprint *astro-ph/0506437*
- Profumo, S., 2005, *Phys. Rev. D*, 72, 103521
- Porter, T., Moskalenko, I.V. & Strong, A.W. 2006, *ApJ*, 648, 29
- Porquet, D., Decourchelle, A., Warwick, R.S., 2003, *A&A*, 401, 197
- Punch, M. (for the H.E.S.S. collaboration), 2005, in *Proc. "Towards a Network of Atmospheric Cherenkov Detectors VII"* (Palaiseau), p 379
- Quataert, E. & Loeb, A., 2005, *ApJ*, 635, L45
- Rolland, L. & Hinton, J. A. (for the H.E.S.S. collaboration), 2005, *Proc. 29th ICRC*, vol 4, p109
- Sidoli, L., Mereghetti, S., Israel, G.L. & Bocchino, F., 2000, *A&A*, 361, 719
- Thompson, D.J. 2004, *New Astron. Rev.*, 48, 543
- Tsuchiya, K., et al., 2004, *ApJ*, 606, L115
- Wang, Q. D., Lu, F. J. & Gotthelf, E. V., 2006, *MNRAS*, 367, 937
- Yusef-Zadeh, F., Wardle, M. & Roverts, D. 1996, *ApJ*, 458, L21
- Yusef-Zadeh, F., 2006, private communication.